PNAS RESEARCH ARTICLE | ENGINEERING PLANT BIOLOGY OPEN ACCESS

eSoil: A low-power bioelectronic growth scaffold that enhances crop seedling growth

Vasileios K. Oikonomou[a,b,1], Miriam Huerta[a,1], Alexandra Sandéhn[a,b,1], Till Dreier[c,d], Yohann Daguerre[e], Hyungwoo Lim[f], Magnus Berggren[a,b], Eleni Pavlopoulou[g], Torgny Näsholm[f], Martin Bech[c], and Eleni Stavrinidou[a,b,e,2]

Edited by Alberto Salleo, Stanford University, Stanford, CA; received March 12, 2023; accepted November 15, 2023 by Editorial Board Member John A. Rogers

Active hydroponic substrates that stimulate on demand the plant growth have not been demonstrated so far. Here, we developed the eSoil, a low-power bioelectronic growth scaffold that can provide electrical stimulation to the plants' root system and growth environment in hydroponics settings. eSoil's active material is an organic mixed ionic electronic conductor while its main structural component is cellulose, the most abundant biopolymer. We demonstrate that barley seedlings that are widely used for fodder grow within the eSoil with the root system integrated within its porous matrix. Simply by polarizing the eSoil, seedling growth is accelerated resulting in increase of dry weight on average by 50% after 15 d of growth. The effect is evident both on root and shoot development and occurs during the growth period after the stimulation. The stimulated plants reduce and assimilate NO_3^- more efficiently than controls, a finding that may have implications on minimizing fertilizer use. However, more studies are required to provide a mechanistic understanding of the physical and biological processes involved. eSoil opens the pathway for the development of active hydroponic scaffolds that may increase crop yield in a sustainable manner.

bioelectronics | electrical stimulation | plant growth

Significance

Hydroponics are used for cultivation of vegetables, leafy greens, and fodder. Areas with limited arable land, poor soil quality, and harsh environmental conditions can benefit from hydroponic food production. Substrates used in hydroponics mainly offer support to the roots. Here, we developed a bioelectronic soil, the eSoil, that provides electrical stimulus on plants' roots and their environment in hydroponics. We show that barley seedlings growth is enhanced as the dry weight increased on average by 50% after electrical stimulation. eSoil consumes little power and its main structural component is cellulose, the most abundant polymer. This work opens the pathway for using physical stimuli to enhance plant growth but also provides a platform to understand better plant responses to electric field.

The world population is currently 7.97 billion and is expected to increase to 9.6 billion by 2050 (1), imposing the need to increase food production by 60% to cover the demands. Hydroponic agriculture is the plant cultivation in soilless media usually in closed controlled environments, and it is mainly used for cultivation of vegetables, leafy greens, microgreens, or fodder. Hydroponics have several advantages over soil cultivation particularly of higher water use efficiency and less use of fertilizers (2, 3). Water use efficiency (WUE), in terms of the amount of harvested product per unit of water supply, is maximized in hydroponics as the water is reused, something that cannot be done in soil cultivation (3, 4). In terms of fertilizer use, hydroponics have also an advantage, as in soil, less than 50% of the nutrients are taken up by the crops (5), while in hydroponics, the nutrient solution can be recirculated in the system. Hydroponics can be integrated in vertical farm configuration, which is compatible with the urban environment, reducing land usage for agricultural purposes and cutting down long-range food transportation costs by bringing the production sites closer to the urban consumers. However, the potential of hydroponics, and (semi-) closed environment agriculture in general, to contribute to food security is not proven yet as it is not currently used for production of major grains (6, 7). Furthermore, there are associated economic and environmental costs related to the energy and materials demands of closed environment agriculture. There are areas where hydroponic agriculture can make a bigger impact such as countries with very little arable land [e.g., Singapore (8)] and areas with low soil fertility or harsh environmental conditions. Low-tech hydroponics systems are also promoted by the Food and Agriculture Organization of the United Nations (FAO) for fodder production in arid and vulnerable locations (9).

Typically, in hydroponics, the roots are suspended in a nutrient solution or supported by a substrate (growth scaffold). Currently the most widely used substate in hydroponics is rockwool; mineral wool, which is not biodegradable and it is produced by an energy intensive process; melting of basaltic rock. Replacing rockwool with biopolymers will significantly contribute to the sustainability aspects of hydroponics culture (10). While the interest in hydroponics is increasing, the current scaffolds mainly provide support to the root system without any other stimulating effect on the plant growth and development. Active hydroponic substrates whose properties can change and provide stimulus on demand or even monitor root processes have not been demonstrated so far, to the best of our knowledge (11–13). Indeed, plants respond to a number of physical stimuli, and while there is great understanding

Author contributions: V.K.O., M.H., A.S., Y.D., M. Berggren, T.N., M. Bech, and E.S. designed research; V.K.O., M.H., A.S., T.D., Y.D., and E.P. performed research; V.K.O., M.H., A.S., T.D., Y.D., H.L., E.P., and E.S. analyzed data; E.S. supervised research and conceived the project; and E.S. wrote the paper.

The authors declare no competing interest.

This article is a PNAS Direct Submission. A.S. is a guest editor invited by the Editorial Board.

[1]V.K.O., M.H., and A.S. contributed equally to this work.

[2]To whom correspondence may be addressed. Email: eleni.stavrinidou@liu.se.

This article contains supporting information online at https://www.pnas.org/lookup/suppl/doi:10.1073/pnas.2304135120/-/DCSupplemental.

Published December 26, 2023.

of plants' responses to light, temperature, and gravity, for example, the response of plants to an electric field is not well understood.

Most studies on plant responses to electric field can be divided into two categories. The first one relates to the phenomenon of electrotropism, where the roots grow along the direction of an electric field. Even though this phenomenon was first observed in the late 19th century, since then, there have been only scattered reports in the literature (14, 15). In studies of electrotropism, an electric field, in the order of a few volts per cm, is applied to the growth medium with the use of metal electrodes (16–19). One of the main limitations of these studies is that it is not clear whether the roots are under the influence of an electric field as they are not in contact with the electrodes, and after the initial polarization of the electrodes, no electric field should be present in the electrolyte. Furthermore, in some of the studies, high voltage is applied between the electrodes that induces electrochemical reactions and generation of reactive species. Another set of works focuses on stimulating plant growth by applying high electric fields reaching a few kV/cm between the plant and the air using metal electrodes. In this case, a high-voltage source is required that has safety considerations, and it is energy demanding while the physics of the system becomes more complicated. Growth enhancement was reported for barley (20), the model plant *Arabidopsis thaliana* (21), and most recently for pea seedlings (22). The growth enhancement was suggested to be related to various physiological processes, yet a clear understanding on how the high electrostatic field is influencing these processes is missing. Nevertheless, it must be noted that in both categories of studies, the effect of the electric field might be indirect, thus affecting the growth environment of the plant rather than the plant processes per se.

In this work, we developed another approach for electrical stimulation of plants, a bioelectronic soil or eSoil, a 3D porous conducting growth scaffold based on an organic mixed ionic electronic conductor (OMIEC) and cellulose. The eSoil overcomes limitations of previous studies: i) the eSoil acts simultaneously as a stimulating electrode and a growth scaffold, and therefore, the root system is under the influence of an electric field during stimulation; ii) the electrical stimulation is based on low voltage with low power consumption; iii) eSoil can be integrated in hydroponic culture and its main structural component is cellulose, the most abundant biopolymer; and iv) the active material is an OMIEC that offers several advantages for interfacing with the biological systems over inorganic counterparts (23, 24). OMIECs are stable in aqueous environments, and due to their mixed conduction, they have a volumetric capacitance that results in electrodes with low impedance for recording and stimulation (23). Furthermore, their oxidation state can be changed via electrochemical doping at low voltages ($V < 1$ V) that also results in a desired tuning of their physicochemical properties (i.e., hydrophilicity, surface pH, volume) (24). OMIECs can be processed from aqueous solutions, and they can even self-organize directly within the biological environment (25, 26) or be processed into various 3D form factors such as porous scaffolds for cell growth (27). We demonstrate that the eSoil can support the growth of barley seedlings and that electrical stimulation increases the dry weight of the seedlings by 50% in hydroponics conditions. The growth enhancement takes place during the growth period after the stimulation, and it is associated with more efficient nitrate assimilation.

Results

eSoil is based on the blend of the conjugated polymer PEDOT:PSS (poly(3,4-ethylenedioxythiophene):polystyrene sulfonate) and carboxymethyated cellulose nanofibrils and is fabricated using the ice templating technique (Fig. 1 *A*–*C*). PEDOT:PSS is a p-type doped OMIEC while nanocellulose is used as the main structural component and to enhance the mechanical properties of the scaffold (28, 29). PEDOT:PSS-NFC solution with carbon fiber bundles, which were added to act as the addressing electrodes of the scaffold, was frozen at −20 °C for 24 h in plastic molds. Ice crystals that are formed in areas between the solutes are then removed via sublimation in a lyophilizer resulting in a porous 3D scaffold (*SI Appendix*, Fig. S1). To improve the water stability of the scaffold, we added in the solution the cross-linker GOPS (glycidoxypropyl trimethoxysilane) whose epoxy groups react with the hydroxyl groups present in PSS and NFC after thermal annealing of the scaffold (30). The amount of the cross-linker can also affect the porosity of the scaffold and its mechanical properties as we have previously demonstrated (31). To increase the electronic conductivity, the scaffold was treated with DMSO vapor that acts as secondary dopant (*SI Appendix*, Fig. S2). It was shown that the DMSO treatment changes the transport mechanism in PEDOT going from hopping mechanism to temperature-independent transport (28). So far, the demonstration of PEDOT and PEDOT-NFC scaffolds has been limited to the sub-cm scale. Here, we developed a scaffold in cm scale in order to be suitable to accommodate the growth of the root system.

The structural organization of dry scaffolds at the subnanoscale was characterized with wide-angle X-ray scattering (WAXS) (*SI Appendix*, Fig. S3). While there is a lot of work on studying the microstructure of PEDOT:PSS and the effect of various additives, not much is known for the microstructure of PEDOT-based porous scaffolds (or aerogels). PEDOT:PSS mixed with cellulose nanofibrils was processed to form a paper-like composite with high electronic and ionic conductivity (32). Microstructural analysis of the PEDOT-NFC paper revealed that PEDOT:PSS organizes by π–π stacking forming bead-like structures along the nanocellulose fibers (33–35). However, the organization of PEDOT and cellulose in porous scaffolds has not been studied to the same extent (36). PEDOT:PSS adopts an ordered structure in the scaffolds with PEDOT-rich and PSS-rich domains, as indicated by the π–π stacking peak of PEDOT at 1.85 $Å^{-1}$ and the amorphous halo peak of PSS at 1.25 $Å^{-1}$, arranged in alternating lamellae (*SI Appendix*, Fig. S3). The presence of a weak (110) cellulose peak at 1.59 $Å^{-1}$ shows that NFC preserves its cellulose structure (35). These observations are in line with the reports on PEDOT:PSS-NFC composites (33, 34). After cross-linking with GOPS, PEDOT chains maintain their organization in π–π stacks. Interestingly, the (100) PEDOT peak shifts to higher q values which suggests a decrease in the PEDOT/PSS lamellar stacking distance, something that favors charge transport between the different PEDOT-rich domains (37). The DMSO treatment does not affect the PEDOT chains organization in ordered π–π stacks. We also attempted to characterize the microstructure of wet scaffolds as it will better reflect the scaffolds used for the plant growth. However, due to significant swelling of the NFC and overlap of its scattering pattern with the PEDOT peaks, we could not observe any contribution from the PEDOT:PSS phase.

While the information at the subnanometer scale is useful for understanding the materials' properties, the morphology of the eSoil is important for the root integration and plant growth. X-ray micro-CT is a powerful method to characterize the internal morphology of porous structures as it can give high-resolution imaging of the whole volume and hence characterization of the bulk properties. The imaging confirmed the porous structure with overall porosity of 87% and the majority of pore size between 50 and 300 μm (Fig. 1 *D* and *E*). The pore size is fairly uniform within the scaffold length with slightly larger- pores toward the upper

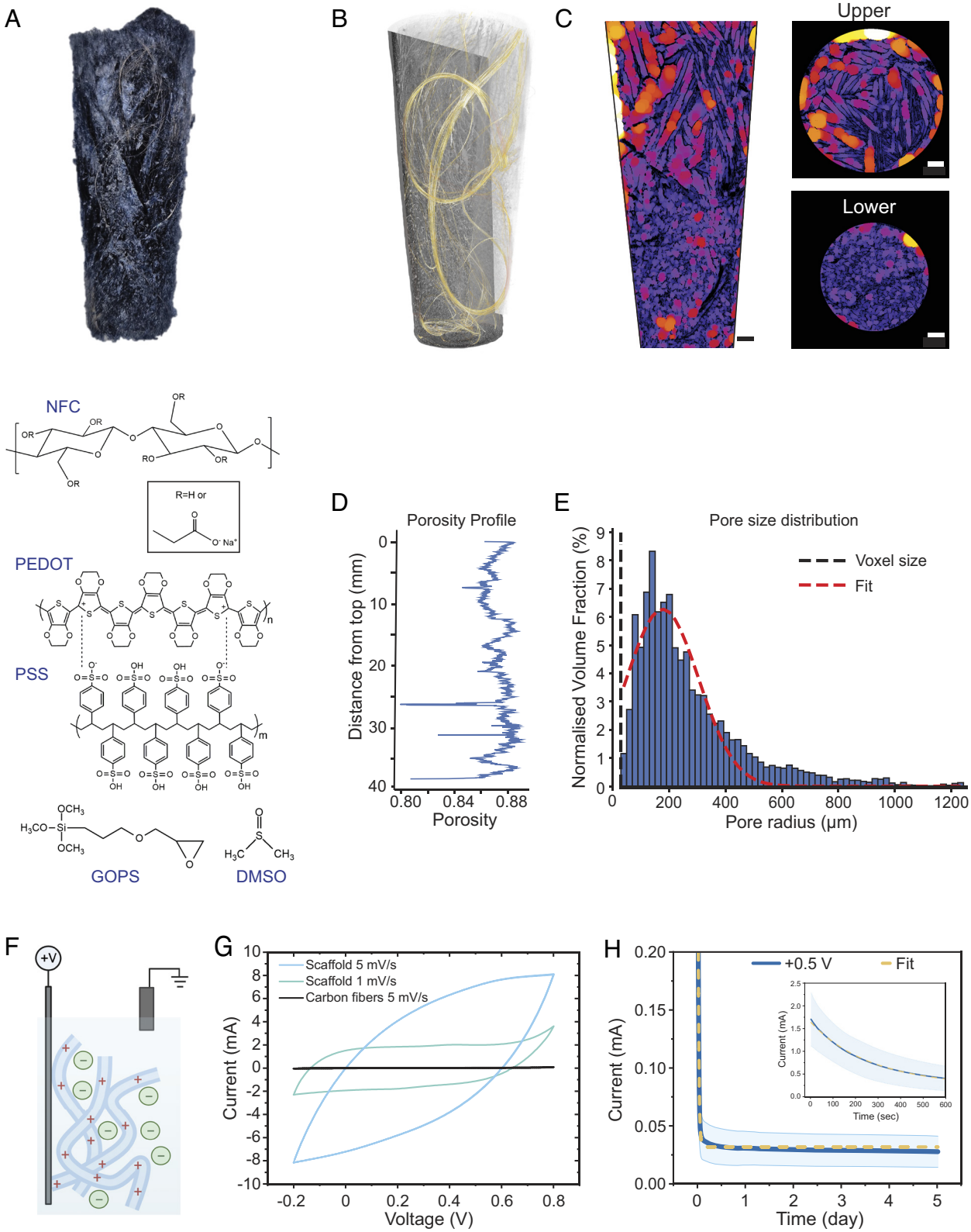

Fig. 1. eSoil: a 3D porous conducting scaffold for plant growth. (*A*) Photograph of the eSoil and the chemical structures of its components; nanofibrillated cellulose (NFC), PEDOT:PSS, GOPS, and DMSO. (*B*) X-ray micro-CT scan of the scaffold (gray) and the carbon fibers (gold). (*C*) Reconstructed orthogonal CT slice through the volume with the local thickness filter applied (bright means larger pore size) and slices from the *Upper* and *Lower* part of the volume showing the difference in pore size (Scale bars, 2 mm). (*D*) Porosity per CT slice through the volume from top to bottom. (*E*) Distribution of pore sizes in the volume showing that the majority of pores have a radius in the range of 50–300 µm, Gaussian fit: FWHM = 306.36 µm. (*F*) Simplified schematic of the eSoil charging during oxidation. Holes (red crosses) are injected from the external electrode (gray) to the PEDOT backbone (blue threads) and compensated by anions (green circles) in the electrolyte. (*G*) Cyclic voltammetry (CV) of scaffolds at different scan rates (5 mV/s and 1 mV/s) and for only the carbon fibers (5 mV/s). (*H*) Chronoamperometry of scaffold over the period of 5 d; the *Inset* shows the current response during the first 10 min. The fit corresponds to a double exponential decay.

part of the scaffold (*SI Appendix*, Figs. S4 and S5). Larger pores appear to have a more elongated shape, while most of the smaller pores are more spherical. In addition, the tomography enables the visualization of the carbon fibers within the bulk of the scaffold showing that the fibers are rather randomly distributed (Fig. 1*B*).

Next, we characterized the electrochemical properties of the eSoil. CV revealed the electroactive nature of the eSoil that is governed by the PEDOT:PSS properties (Fig. 1 *F* and *G*). When negative voltage is applied on eSoil in respect to the electrolyte potential, PEDOT:PSS is electrochemically reduced or dedoped as holes (polarons/bipolarons) are extracted from the polymer backbone and cations are injected into the polymer matrix to compensate the negative charges on the PSS and maintain the electroneutrality of the system. On the other hand, when a positive voltage is applied to the eSoil, PEDOT is oxidized with holes being injected into the polymer backbone and either cations are expelled, or anions enter into the polymer matrix to compensate the accumulated charges (Fig. 1*F*). CV shows that indeed the nature of charging is capacitive for a low scan rate of 1 mV/s within the voltage range of (−0.1, +0.5 V) (Fig. 1*G*). This agrees with the current understanding of PEDOT:PSS doping processes that are dominated by electrostatic interaction between ions and the electronic carriers on the PEDOT backbone (38, 39). However, for higher scan rates, the resistive components dominate due to ionic or even electronic transport limitations (40). Chronoamperometry revealed that the eSoil charging at V_{appl} = 0.5 V has two time constants, a fast charging component with characteristic time of t_1 = 4 min and a second one with t_2 = 26 min (Fig. 1*H* and *SI Appendix*, Fig. S6). Even for long time operation, up to 5 d, current in the order for tens of microamps is still sustained in the system.

To demonstrate the applicability of the eSoil platform, we developed a simplified hydroponic setup to study the plant growth. We selected barley (*Hordeum vulgare cv. 'KWS Irina'*) as the plant model system as it is grown hydroponically for green fodder production. First, to evaluate the suitability of the eSoil as a plant growth scaffold, without any electrical stimulation, we compared the growth of plants in eSoil with plants grown in rockwool a common substrate used in hydroponics.

eSoil scaffolds were fabricated and then electrochemically cycled and rinsed in DI water (*Materials and Methods*) to remove any excess additives that might be harmful for the plant such as DMSO (*Materials and Methods* and *SI Appendix*, Fig. S7). eSoil and rockwool substrates were then placed in open containers filled with ½ Murashige and Skoog (MS) medium and placed in a growth chamber with controlled light, humidity, and temperature. Randomly selected pregerminated seeds were placed on the surface of the substrates, eSoil or rockwool, and the plants were let to grow for 15 d (Fig. 2*A*). For each plant, a separate container was used (Fig. 2*A*). At 15 d postgermination, the plants were harvested, and their phenotype was characterized (Fig. 2*B*). The plants grown in rockwool had a mean dry weight of 0.075 ± 0.0095 g (n = 5), and the plants in eSoil had a mean dry weight of 0.06 ± 0.005 g (n = 6; Fig. 2 *C* and *D*). Overall, the difference in growth between rockwool and eSoil in dry weight or length was not statistically significant; however, we point out that we used a relatively small number of samples in this experiment.

No visible sign of contamination such as mold was observed; however, we have not performed any microbiology analysis. The root system distribution within eSoil was visualized with X-ray micro-CT in freeze-dried samples after 15 d of growth. The roots were well integrated within the porous matrix with no preferential distribution (Fig. 2 *E*–*G*). In addition, scanning electron microscopy revealed the close interaction of the roots with the conducting matrix, with the roots growing within the pores of the scaffold and even the root hairs penetrating the polymer wall (Fig. 2*G*). Overall, the data suggest that the eSoil is a good substrate for plant growth and the intimate interaction between the roots and the conducting scaffold material can be leveraged for electrical stimulation.

Next, we proceed to electrically stimulate the root system via the eSoil and study the effect on the plant growth (Fig. 3). Enhancement of plant growth upon electrical stimulation was reported so far for plants growing under high electric field (in the order of few kV/cm), applied between plant and air. The eSoil platform is fundamentally different as it serves simultaneously as a stimulating electrode and a growth scaffold. Here, we leveraged the conducting nature of the scaffold that enables application of low electric field within the safe electrochemical window of PEDOT:PSS. As there is no precedent on electric field stimulation of plants via an integrated conductor, we performed preliminary experiments to guide us on the selection of the stimulation protocol (*SI Appendix*, Fig. S8). One of the main considerations was to operate the eSoil in the PEDOT capacitive region, i.e., in the charge polarization regime to avoid electrochemical side reactions and to be well below the electrolysis regime (*SI Appendix*, Fig. S9). Based on the preliminary experiments, we proceeded to investigate in more detail the stimulation with constant voltage +0.5 V for 5 d (Fig. 3).

Five-day-old plants growing within the eSoil were stimulated for five days and then grew for an additional five days prior to harvest (Fig. 3 *A*–*C*). Remarkably, the growth of stimulated plants was enhanced in comparison with the controls. In all independent experiments (n = 5) the same trend was observed, although with variations in the absolute values. The mean length of control plants was 21.9 ± 2.9 cm while of stimulated plants was 28.8 ± 2.9 cm resulting in an overall increase of length by 31.5% (Fig. 3*D*). The enhanced growth of the stimulated plants was reflected in the dry weight as well with mean dry weight of control plants equal to 0.074 ± 0.016 g and the one of stimulated plants equal to 0.111 ± 0.015 g resulting in an average increase of dry weight by 50% (Fig. 3*E*). We also observed that in some cases the stimulated plants produced more leaves than controls (*SI Appendix*, Fig. S10). However, from these sets of experiments, it was not clear when in time the electro-activated impact on the growth took place. Therefore, we performed a new set of experiments where we harvested plants at different time points: i) at day 5: before applying stimulation, ii) at day 10: right after the end of the stimulation period, and iii) at day 15: 5 d after the end of stimulation (Fig. 4). Surprisingly, these results showed that the growth enhancement did not take place right after the end of stimulation (day 10), but when the plants were allowed to grow for an additional five days. At day 10, the mean dry weight of the control plants was 0.052 ± 0.002 g while the one of stimulated plants was 0.051 ± 0.008 g (Fig. 4*C*). Overall, we observed higher growth changes in the second growth period, between day 10 and 15 for the stimulated plants in comparison with the controls (Fig. 4*D*). Although the electrical stimulus was applied to the root system, root:shoot ratio of biomass between control and stimulated plants was not significantly different, suggesting a comparable growth enhancement at both root and shoot levels (*SI Appendix*, Table S2).

After validating the positive effect of the stimulation on the plant growth, we tested whether the stimulation is specific to the polarity of the applied voltage. We performed experiments where we applied −0.5 V for 5 d mirroring the protocol we used previously. In this case, growth of the two treatments was not significantly different (*SI Appendix*, Fig. S8*C*). We investigated whether in this case, reactive species are produced due to the oxygen

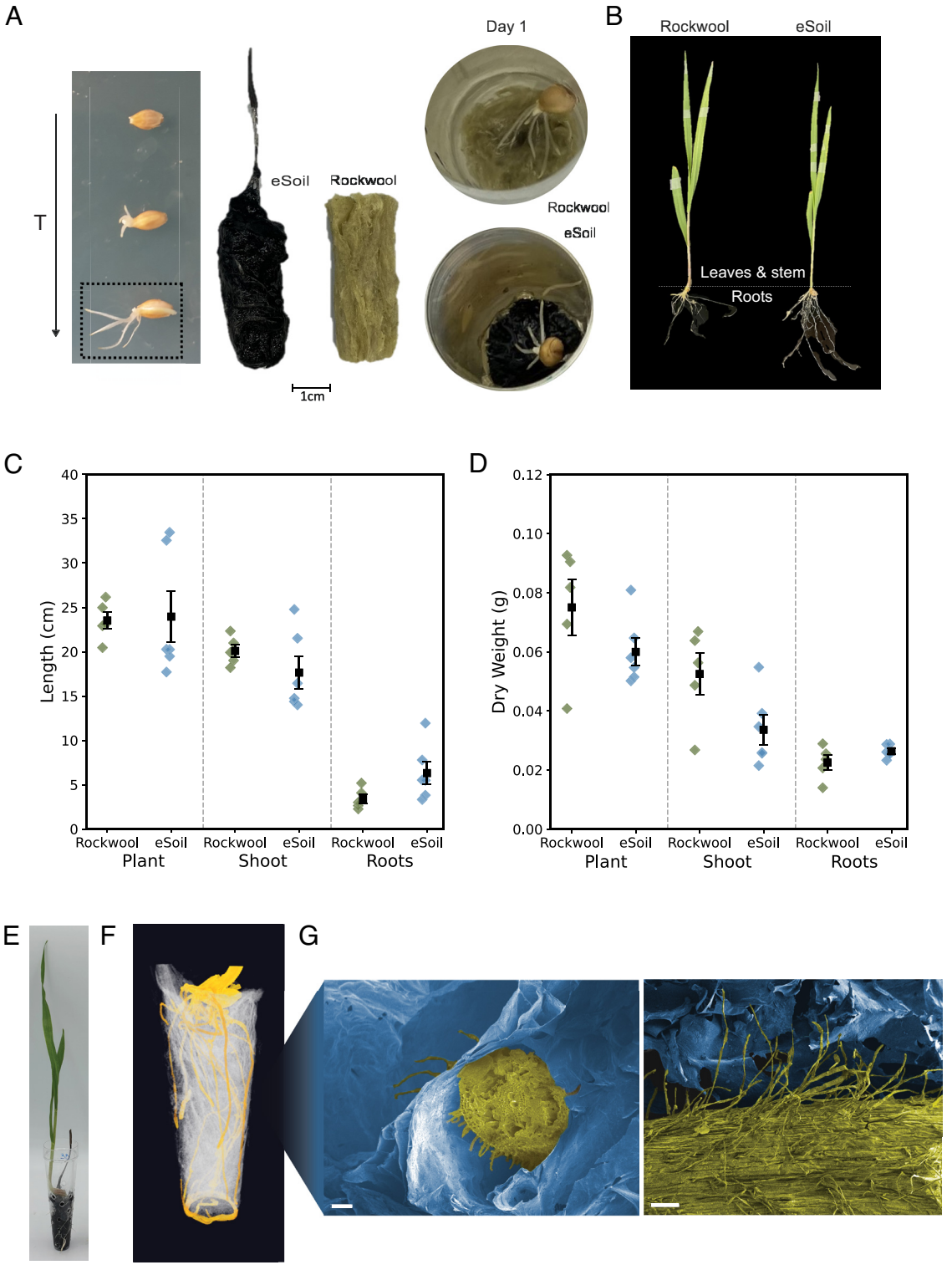

Fig. 2. eSoil supports the growth of the root system with plants growing as well as in rockwool in hydroponics. (*A*) Experimental setup for the plant growth assay in rockwool and eSoil. Pregerminated seeds are placed in rockwool or the eSoil and let to grow for 15 d in individual containers for each plant. (*B*) Photograph of the plants grown in rockwool and eSoil at the time of harvest. (*C*) Length of the plant, shoot, and main root after 15 d of growth in rockwool ($n = 5$) and eSoil ($n = 6$). Mean value and SE are depicted with the black square. No significant statistical difference between rockwool and eSoil (Dataset S1). (*D*) Dry weight of the plant, shoot, and tap root after 15 d of growth in rockwool ($n = 5$) and eSoil ($n = 6$). Mean value and SE are depicted with the black square. No significant statistical difference between rockwool and eSoil (Dataset S1). (*E*) Photograph of a barley plant after 15 d of growth in eSoil. (*F*) X-ray micro-CT of the plant showing the seed with the roots of the barley (yellow) and eSoil (white). (*G*) SEM micrographs of the roots (yellow) growing through and along the eSoil (blue) (Scale bars, 100 μm.) Details for statistical analysis are given in *Materials and Methods*.

reduction reaction at cathodic potentials on PEDOT (41, 42). However, analysis of the medium with a H_2O_2 colorimetric enzymatic assay did not show any presence of the H_2O_2 within the detection limit of the assay used (*SI Appendix*, Fig. S11).

Even if the enhanced growth is obvious when eSoil is positively polarized, it is not clear how the electrical stimulation affects the plant's physiological processes. One hypothesis is that the growth boost is a result of a more efficient nutrient uptake from the growth

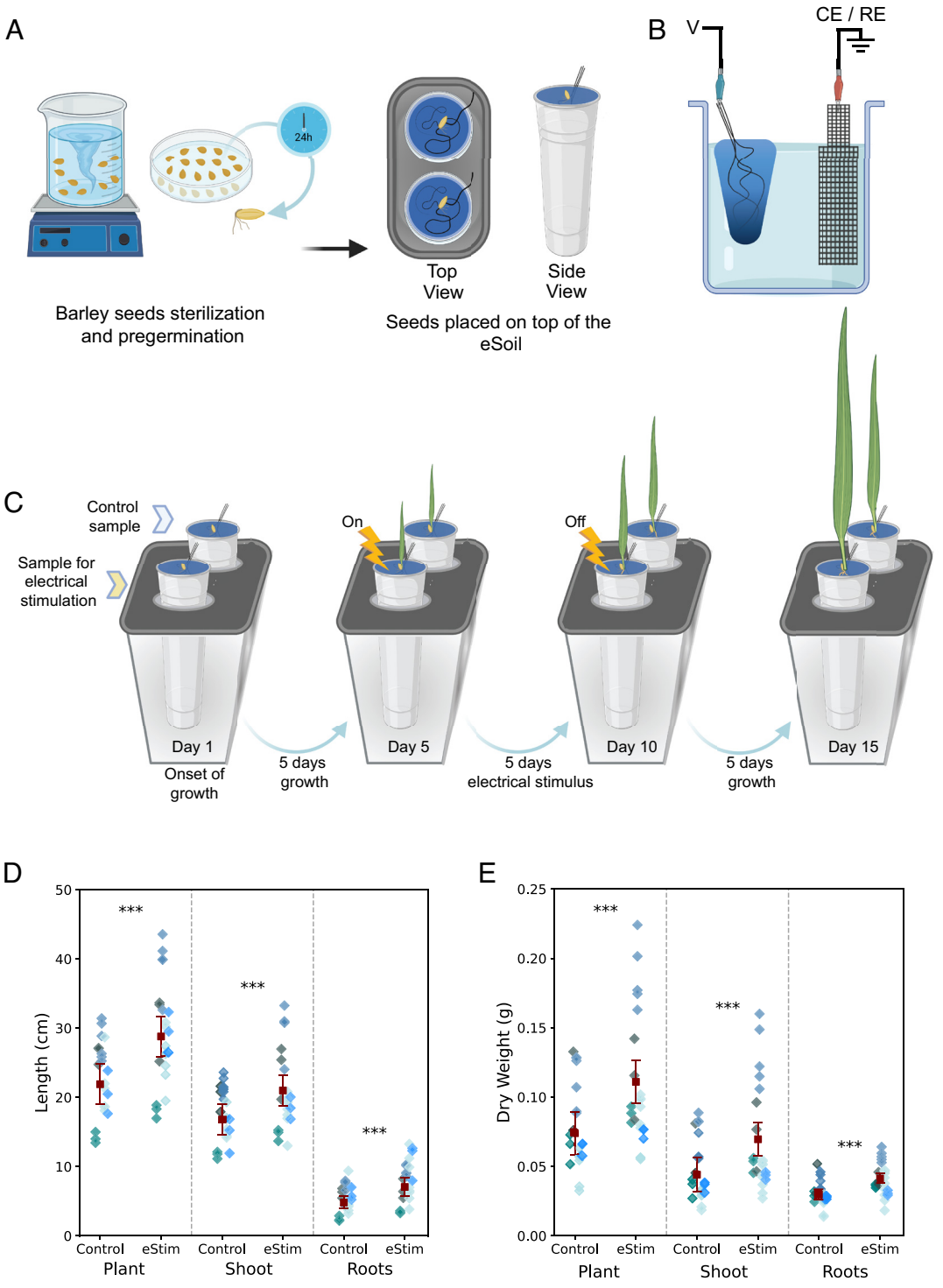

Fig. 3. Electrical stimulation via eSoil enhances plant growth in hydroponics conditions. (*A*) Seed sterilization and pregermination protocol. Randomly selected seeds are placed on eSoil (one seed per scaffold) for control and stimulation samples. Each eSoil has its own electrolyte compartment. (*B*) Electrical stimulation setup where voltage is applied at eSoil in respect to the electrolyte. (*C*) Schematic for the plants' growth and electrical stimulation protocol where plants are stimulated between days 5 and day 10 and are harvested at day 15 for analysis. (*D*) Length of the plant, shoot, and main root after 15 d of growth in eSoil with and without electrical stimulation ($n_{Control}$ = 21, n_{eStim} = 23) (Dataset S2). (*E*) Dry weight of the plant, shoot, and main root after 15 d of growth in eSoil with and without electrical stimulation ($n_{Control}$ = 20, n_{eStim} = 23) (Dataset S2). The different colors correspond to independent experiments. Mean estimates and their SEs are depicted with the red square, and * corresponds to the *P* values where **P* values <0.05 were considered significant; ** sets for *P* values < 0.01 and *** for *P* values < 0.001; details of the statistical analysis are given in *Materials and Methods*.

medium. It is well known that one limiting process for root uptake is the diffusion of nutrients toward the root surface (43, 44). This process in natural environments is driven by the concentration gradient of the nutrients between the root surface and the growth medium and in most situations, nitrogen acquisition is the limiting factor for plant growth. When eSoil is positively polarized, PEDOT:PSS is electrochemically oxidized, resulting in expulsion of cations and accumulation of anions from the electrolyte into the bulk of the polymer to compensate the extra charges on the PEDOT backbone (45). To test this hypothesis and track any possible change

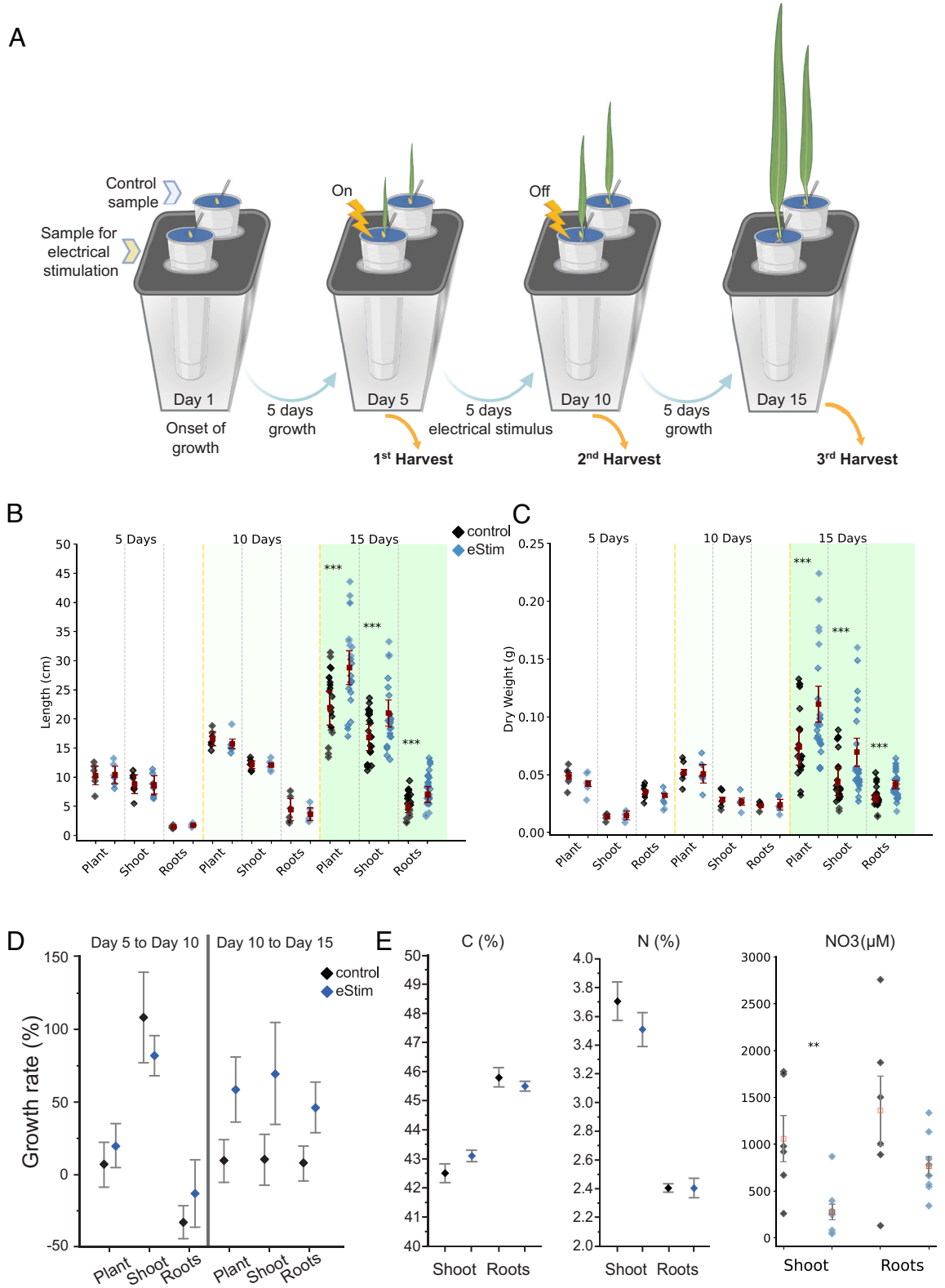

Fig. 4. Growth enhancement takes place during the growth period after the end of the electrical stimulation. (*A*) Schematic of the plant growth and electrical stimulation protocol where plants are stimulated between day 5 and day 10 and are harvested at days 5, 10, and 15 for analysis. (*B*) Length of the plant, shoot, and main root after 5, 10, and 15 d of growth in eSoil for control and stimulated plants (the red square represents mean estimates, and error bars represent the SEM estimates. N values: 5 d: $N_{Control}$ = 6, N_{eStim} = 6; 10 d: $N_{Control}$ = 6, N_{eStim} = 6; 15 d: $N_{Control}$ = 21, N_{eStim} = 23 (Dataset S2). (*C*) Dry weight of the plant, shoot, and main root after 5, 10, and 15 d of growth in eSoil for control and stimulated plants (the red square represents mean estimates, and error bars represent the SEM estimates). N values: 5 d: $N_{Control}$ = 6, N_{eStim} = 6; 10 d: $N_{Control}$ = 6, N_{eStim} = 6; 15 d: $N_{Control}$ = 20, N_{eStim} = 23 (Dataset S2). (*D*) Growth rate between days 5–10 and days 10–15 for control and stimulated plants. Growth rate is defined as the increase in biomass for the 5-d period. $N \geq 6$. (*E*) Root and shoot carbon and nitrogen % composition and NO_3^- content at day 15 $N_{Control}$ = 6, N_{eStim} = 9 (Dataset S3) (* corresponds to the *P* values < 0.05 that were considered significant; ** for *P* values < 0.01 and *** for *P* values < 0.001. Details of the statistical analysis are given in *Materials and Methods*).

in the plants' nitrogen status and nitrogen uptake rates, barleys were cultivated in eSoil within a nutrient solution containing 1 mM NO_3 enriched with 2 atom% ^{15}N. The electrical stimulation was applied between day 5 and day 10 while samples were harvested and analyzed for total nitrogen and ^{15}N content at day 15. The analysis revealed no significant difference in the overall nitrogen status of roots and shoots over time, as well as no significant increase in the uptake of the labeled nitrogen due to the stimulation (Fig. 4*E* and *SI Appendix*, Table S3). This suggests that NO_3^- absorption by the root and nitrogen allocation to the shoot through xylem loading are neither positively nor negatively affected by the electrical stimulation. The carbon status of the plant was also not affected by the electrical stimulation.

A second hypothesis was that the electrically stimulated plants are metabolically more efficient in converting NO_3^- into nitrogen-containing biomass compared to the control. In order to test this hypothesis, we repeated the assay above and analyzed the NO_3^- content of the 15-d-old plants using a colorimetric assay (adapted from ref. 46). Stimulated plants showed in general lower NO_3^- concentration as compared to control plants (Fig. 4*E*), corroborating the hypothesis that the stimulated plants reduced assimilated NO_3^- more efficiently than the nonstimulated ones. This process can potentially lead to a higher biomass production as we observed in the stimulated plants. The molecular mechanisms underlying this phenomenon as well as the behavior of organic nitrogen sources such as arginine and glutamine will be further investigated in the future.

Finally, we tested whether the application of electrical stimulation is inducing physicochemical changes in the growth solution by monitoring temperature, pH, and dissolved oxygen levels over 15 d in control and stimulation experiments. We observed that T, pH, and DO levels remain constant over the duration of the experiment without any notable change due to the application of the stimulation voltage (*SI Appendix*, Fig. S12).

Conclusions

In conclusion, we developed a bioelectronic growth scaffold, the eSoil, that enhances barley seedling growth in hydroponics on average by 50% after application of electrical stimulation. The growth enhancement is obvious both to root and shoot and occurs during the growth period after the electrical stimulation signifying that the stimulation is not just inducing a momentary effect, but it triggers processes that eventually change the plant development. This indicates that the beneficial effect can be achieved via a stimulation treatment without the need of a continuous stimulation throughout the plant growth. However, our work focused on seedlings, and therefore, more studies are required to show whether growth enhancement by stimulation treatment at the early stages of growth impacts the whole growth cycle of plants. The physical processes that take place during the scaffold polarization can be described by the steady state and transient response. When the eSoil is polarized, we observe a fast transient charging process corresponding to 87 mC and then a slow phase of almost constant current resulting in total charge of 14 C. We operate the scaffold at +0.5 V where mainly capacitive processes take place. However, it is not clear whether the slow phase can be associated with capacitive charging or to any associated faradaic reactions. The sustained current flow however indicates that an electric filed is present not only at the electrode/electrolyte interface but also in the electrolyte throughout the duration of the stimulation, thereby influencing the whole root system. For comparison, we performed chronoamperometry in eSoil without DMSO treatment and observed similar charging for +0.5 V for 5 d resulting in total charge of 15 C (*SI Appendix*, Fig. S13). This indicates that the DMSO treatment to enhance the conductivity of the eSoil might not be crucial for DC stimulation.

To elucidate the induced biological processes first, we tested the hypothesis that anionic nutrients such NO_3^- migrate toward the eSoil polymer wall and therefore come in closer proximity to the roots for uptake. However, our analysis revealed that the stimulated and control plants had similar NO_3^- uptake. Regardless, we found that the reduction of assimilated NO_3^- was more efficient in the stimulated plants, a finding that can have implications on minimizing the use of fertilizers. Even though we do not have a clear hypothesis on how the electric field is influencing the nitrogen assimilation, we observed that the beneficial effect of the stimulation depends on the polarity of the voltage, indicating a strong correlation to the electric field distribution. While more studies are required to provide a mechanistic understanding on the physical and biological processes involved, the eSoil can act as a model stimulation system to elucidate the molecular mechanisms that underpin the plant responses to electric field stimulation. Furthermore, by varying the scaffold's composition and its properties such as mechanical properties, morphology–porosity, and biofunctionalization, the platform can be extended for studying the effect of physical and chemical stimuli on root development and ultimate plant growth. For eSoil to be relevant for large-scale applications in closed environment agriculture, there are many aspects to be considered. One of the benefits of our approach in comparison with other works is that the eSoil is a low-power device (power consumption in the μW order) and can be in principle powered with photovoltaics. As barley is also used as fodder, higher biomass at the young age of the plant will enable feeding more feedstock with the same resources. We hope that our work will open a broad avenue of research for material science-based solutions for active hydroponics scaffolds that may increase crop yield in a smart and sustainable manner.

Materials and Methods

eSoil-Conducting Porous Scaffold Fabrication. PEDOT:PSS-NFC-GOPS scaffolds were prepared as described before (47) with a few modifications. Briefly, PEDOT:PSS (PH1000, 1.3 wt% PEDOT:PSS, Heraeus Clevios), NFC (1 wt% carboxymethylated nanofibrillated cellulose, RISE Innventia), and GOPS (97 wt%, Alfa Aesar) in a ratio of 1:1:0.2, respectively, were homogenized with a disperser (IKA 3386000 ULTRA-TURRAX s). The mixture was poured in 30-mL polystyrene conical containers that contained approximately 0.093 g carbon fibers with an average length of 12.5 cm that were randomly dispersed in the container (PAN-CF Carbon fibers, Hexcel, diameter 7 μm). The container was frozen at −20 °C for 24 h, followed by freeze-drying (BenchTop Pro, SP SCIENTIFIC) under −50 °C and 200 μbar for 72 h. Freeze-drying removes the ice crystals resulting in the formation of a porous soil-like scaffold (Dimensions: Height = 5 cm, $Top_{diameter}$ = 2 cm, $Bottom_{diameter}$ = 1 cm). The scaffolds were then annealed at placed at 140 °C for 30 min to enable the thermal cross-linking of PEDOT:PSS-NFC with GOPS. Finally, the scaffolds were treated with DMSO vapor to enhance their electrical conductivity. The scaffolds were placed in a glass petri dish with a few drops of DMSO aside (1 mL); the petri dish was capped and placed on a hot plate at 60 °C for 24 h.

Scanning Electron Microscopy. The freeze-dried scaffolds (pieces of ~1 cm in diameter) were attached on the sample holder with the help of copper tape. The SEM analysis took place with both InLens and SE2 lens of Zeiss-Sigma 500 Gemini SEM (2–2.5 kV), without any metal evaporation or sputtering.

X-Ray Micro-CT. The used X-ray micro-CT setup (48) consists of a microfocus prototype source with a Tungsten anode using an acceleration voltage of 70 kV from Excillum AB. Images are acquired using a Medipix3-based (49) Lambda350k detector with a 500-μm Gallium Arsenide (GaAs) sensor from X-Spectrum GmbH. The detector has 516 × 772 pixels with a size of 55 μm giving a sensitive area of 28.38 × 42.68 mm^2. The detector is placed 0.55 m from the source; the sample

position was selected to cover the full width of the sample resulting in voxel sizes in the range of 30–35 μm.

Scans are executed with 1080 projections and 1 s exposure time per projection running the source at 30 W emission power focused to a 10 μm X-ray spot. Tomographic reconstructions are performed using the ASTRA toolbox (50, 51) via Python using the Feldkamp–Davis–Kress (FDK) (52) algorithm for cone beam geometry. Additionally, a wavelet ring filter is applied (53). The area around the samples and the plastic container were removed from the 3D volumes, and a radial bias field correction was applied to correct intensity variations in the reconstructed slices.

Segmentations were performed in Amira (Thermo Fischer Scientific). Carbon fibers were segmented using a tubeness filter, which was calculated using a Fiji plugin (54). Porosity analysis is performed in Python using the PoreSpy package (55). The volumes are binarized using Otsu's threshold method (56). Space occupied by fibers and roots is masked using the exported labels volume from Amira. The porosity can be calculated, given as fraction of empty space in the full subvolume or per individual slice. The pore size distribution (57) is calculated by applying a local thickness filter to the volume fitting spheres into the empty space.

Electrochemical Characterization. CV was performed on the scaffolds and carbon fibers in 0.01 M KCl electrolyte (Sigma-Aldrich) at 1 and 5 mV s^{-1} scan rate, between −0.2 and 0.8 V using a metallic mesh as a counter electrode and an Ag/AgCl electrode as a reference electrode. Chronoamperometry was performed on the scaffolds in the same setup as CV by applying a constant voltage was applied over the period of 5 d. All the measurements were performed at room temperature using a Gamry 1010E/B potentiostat.

Plant Growth. Barley seeds (*Hordeum vulgare*) (kindly provided by Scandinavian Seed AB) were surface-sterilized with a 4 % sodium hypochlorite solution for 10 min followed by three rinses, 10 min, with sterile deionized water in constant stirring. To synchronize germination, the cleaned seeds were stored at 4 °C for 7 d before seeding (hibernated seeds). The hibernated seeds were placed on top of a thin layer of ½ Murashige and Skoog (MS) agar pH 5.6 in a petri dish and incubated at 24 °C/18 °C in the darkness for 48 h to pregerminate.

eSoil Rinsing. The scaffolds were rinsed in two steps: The first rinsing step was electrochemical under CV. CV was performed on the scaffolds in 0.01 M KCl electrolyte (Sigma-Aldrich) at 5 mV s^{-1} scan rate, between −0.2 and 0.8 V using a metallic mesh as a counter electrode and an Ag/AgCl electrode as a reference electrode. Then, the second rinse step took place where the scaffolds were rinsed three times with sterile diH_2O for 1 h with constant stirring.

Growth in Hydroponics Setup in eSoil and Rockwool. The eSoil scaffolds were fabricated and rinsed as described above. Rockwool was purchased from HydroGarden. Randomly selected pregerminated seeds were placed on top of the eSoil or Rockwool, and each eSoil or Rockwool was placed in its own open container with sterile ½ MS liquid medium. For the stimulation experiments only eSoil scaffolds were used, both for control and eStim samples. Each container of control or eStim sample included a metallic mesh, but only in the eStim samples voltage was applied during the electrical stimulation. The open containers were placed in a growth chamber with a photon flux density of 100 μmol m^{-2} s^{-1} at 24 °C/18 °C and 12 h light/12 h dark cycles for 15 d (unless stated otherwise).

Electrical Stimulation. Barley grew in the scaffolds for 5 d. Voltage was applied to the eSoil in respect to the electrolyte (½ MS liquid medium) using a Gamry 1010E/B potentiostat or power source. After the stimulation, the plants were let to grow for an additional 5 d. For the experiments with three harvesting periods, a batch of the plants was harvested at day 5 prior to electrical stimulation, the next batch of plants was harvested after the electrical stimulation at day 10, and the last harvest took place at day 15 for the rest of the plants. The analysis of the plants took place after each harvest. When ^{15}N uptake rate needed to be calculated in roots and shoots, 2% of $K^{15}NO_3$ 98% enriched was added to the ½ MS liquid medium, the final KNO_3 concentration being 1 mM.

^{15}N uptake Rate and Total Nitrogen and Carbon Content Measurement. Root and shoot samples harvested at day 15 were dried in the oven at 50 °C for 48 h, bead milled into fine powder, dried in the oven at 60 °C for an additional 72 h, and stored in a desiccator until further use. Using a precision scale, 3 mg of powder per sample was packed in tin capsule and analyzed to determine nitrogen isotope ratios and C and N mass fractions using the Elemental Analyzer–Isotope Ratio Mass spectrometer (EA-IRMS) from the SLU Stable Isotope Laboratory in Umeå, Sweden. The ^{15}N uptake rate (μmol/g dry biomass) was calculated using the nitrogen isotope ratios and the total nitrogen content of the samples.

Root and Shoot Nitrate Content. Nitrate in the roots and the shoots was quantified using a colorimetric assay adapted from the method described by Miranda et al. (46). Briefly, 6 mg of powder per sample was extracted with 80 μL of methanol 20% for 24 h at 4 °C. Then, samples were centrifuged for 10 min at 4 °C at 14,000 rpm, and the supernatant was aliquoted. Nitrate present in the supernatant was reduced to nitrite by adding 20 μL of vanadium (III) chloride to 20 μL of sample. The nitrite generated was revealed by adding successively 20 μL of sulphanilamide and 20 μL of α-NEDD. After 20 min of color development, absorbance at 540 nm was measured. Sample nitrite background was quantified and taken into account by replacing the vanadium (III) chloride by hydrochloric acid.

Morphological Characterization. We measured the length and width, as well as wet and dry biomass of barley plants' growth at different conditions. At the end of each experiment, barley plants were removed from rockwool, or eSoil, and the roots were rinsed with tap water to eliminate all the residues. We divided the plant analysis into three sections: i) shoot that includes the leaves and stem, from the beginning of the stem to the tip of the longest leaf; ii) main root; and iii) plant, that was the sum of the shoot and main root values (Fig. 2*B*). To measure the length, we took digital photographs of the samples with a scale. Using the ImageJ software, we set a scale based on pixels, and then, we obtained the values for the measurements in cm. After removing from rockwool and eSoil, the samples were weighed on an analytical balance (wet biomass), and then they were placed on absorbent towels at 50 °C for 48 h, to remove the water, and weighed again (dry biomass).

Statistical Analysis. The effects of treatment on plants' length and dry mass were determined using a two-sample *t* test, Mann–Whitney *U* test, or a linear mixed model depending on data normality and the experimental design. For comparison between the Rockwool vs. eSoil (Fig. 2), of which experimental design follows a completely randomized design, we checked the normality assumption using the observed data for each group, visually based on a quantile–quantile plot (*SI Appendix*, Fig. S14) and residual distribution against predicted values, and quantitatively based on a Shapiro–Wilk test ($P < 0.05$). We then tested equality of variance between the group, using a F-test ($P < 0.05$) to infer variance equality for performing a two-sample *t* test. When the normality assumption was violated, we performed a Mann–Whitney *U* test to compare the mean difference between the two groups ($P < 0.05$). The stimulation experiments were composed of five independent experiments, but unbalanced sample sizes, so following a randomized block design. We examined the effects using a linear mixed model by treating the experiment as a random effect (block):

$$Y_{ijk} = a + b \times T_j + \varepsilon_k + \varepsilon_{ijk}, \quad [\mathbf{1}]$$

where Y_{ijk} is the response variable in the *i*th plant under *j*th treatment *T* (*j* = control or eStim) with *k*th experiment. *a* is the intercept, *b* is the coefficient to be estimated, ε_k is the random residuals associated with block, and ε_{ijk} is the final residuals. The final residuals were checked for the normality assumption, and when the assumption was unsatisfied, we log-transformed the response variable. Results of normality check for a *t* test and a linear mixed model are given in *SI Appendix*, Figs. S14–S16. Means and their uncertainties were estimated based on the model outcomes, and the relative effect size was computed based on the five experiments ($n = 5$). Statistical analyses were performed using R (v. 4.2.2): The lme function in the nlme package was used for the mixed model (Eq. **1**); lsmeans functions in the lsmeans package were used to compute the mean and SE of the estimates. The R-code used for the analysis is given in *SI Appendix*.

Data, Materials, and Software Availability. All study data are included in the article and/or supporting information.

ACKNOWLEDGMENTS. This work was supported by The Wallenberg Wood Science Center (KAW 2018.0452), the European Union's Horizon 2020 research and innovation program under Grant Agreement No. 800926 (FET-OPEN-HyPhOE), by the Swedish Research Council (VR-2017-04910 and VR 2022-03507) and by the Swedish Foundation for Strategic Research

(FFL18-0101). Additional funding was provided by the Swedish Government Strategic Research Area in Materials Science on Advanced Functional Materials at Linköping University (Faculty Grant SFO-Mat-LiU No. 2009-00971). X-ray scattering experiments were performed at the NCD-SWEET beamline of ALBA synchrotron with the collaboration of ALBA staff and in particular of Dr. Eduardo Solano and using FORTH's laboratory-based SAXS/WAXS XEUSS 3.0 beamline (XENOCS), which was fully funded by the Hellenic Foundation for Research and Innovation (H.F.R.I.) under the "1st Call for H.F.R.I. Research Projects to support Faculty members and Researchers and the procurement of high-cost research equipment" (Project SAXS-SOFT, Project Number: 3401). We thank Renee Kroon, Linköping University, for the NMR analysis, Gwennaël Dufil, Linköping University, for help with data analysis, and Arman Molaei, Linköping University, for help with the T and DO sensors.

Author affiliations: [a]Laboratory of Organic Electronics, Department of Science and Technology, Linköping University, SE-60174 Norrköping, Sweden; [b]Wallenberg Wood Science Center, Department of Science and Technology, Linköping University, SE-60174 Norrköping, Sweden; [c]Department for Medical Radiation Physics, Clinical Sciences Lund, Lund University, SE-22242 Lund, Sweden; [d]Excillum AB, SE-16440 Kista, Sweden; [e]Umeå Plant Science Centre, Department of Forest Genetics and Plant Physiology, Swedish University of Agricultural Sciences, SE-90183 Umeå, Sweden; [f]Department of Forest Ecology and Management, Swedish University of Agricultural Sciences, SE-90183 Umeå, Sweden; and [g]Institute of Electronic Structure and Laser, Foundation for Research and Technology—Hellas, 71110 Heraklion, Crete, Greece

1. A. J. Challinor *et al.*, A meta-analysis of crop yield under climate change and adaptation. *Nat. Clim. Change* **4**, 287–291 (2014).
2. P. Pinstrup-Andersen, Is it time to take vertical indoor farming seriously? *Glob. Food Sec.* **17**, 233–235 (2018).
3. P. Sambo *et al.*, Hydroponic solutions for soilless production systems: Issues and opportunities in a smart agriculture perspective. *Front. Plant Sci.* **10**, 923 (2019).
4. M. Rufí-Salís *et al.*, Recirculating water and nutrients in urban agriculture: An opportunity towards environmental sustainability and water use efficiency? *J. Clean. Prod.* **261**, 121213 (2020).
5. L. Lassaletta, G. Billen, B. Grizzetti, J. Anglade, J. Garnier, 50 year trends in nitrogen use efficiency of world cropping systems: The relationship between yield and nitrogen input to cropland. *Environ. Res. Lett.* **9**, 105011 (2014).
6. D. T. Armanda, J. B. Guinée, A. Tukker, The second green revolution: Innovative urban agriculture's contribution to food security and sustainability–A review. *Glob. Food Sec.* **22**, 13–24 (2019).
7. N. Cowan *et al.*, CEA systems: The means to achieve future food security and environmental sustainability? *Front. Sustain. Food Syst.* **6**, 891256 (2022).
8. J. Ann, E. Sweeney, B. Wong, C. Sian, H. Yao, Feeding cities': Singapore's approach to land use planning for urban agriculture. *Glob. Food Sec.* **26**, 100377 (2020).
9. Food and Agriculture Organization of the United Nations. Food alternative fodder production for vulnerable herders in the West Bank. Food and Agriculture Organization. https://www.fao.org/in-action/kore/good-practices/good-practices-details/en/c/461626/. Accessed 28 June 2023.
10. S. E. Allaire, J. Caron, C. Ménard, M. Dorais, Potential replacements for rockwool as growing substrate for greenhouse tomato. *Can. J. Soil Sci.* **85**, 67–74 (2005).
11. L. M. Kalossaka, G. Sena, L. M. C. Barter, C. Myant, Review: 3D printing hydrogels for the fabrication of soilless cultivation substrates. *Appl. Mater. Today* **24**, 101088 (2021).
12. Y. Hitti, J. Chapelat, B. Sen Wu, M. Lefsrud, Design and testing of bioreceptive porous concrete: A new substrate for soilless plant growth. *ACS Agric. Sci. Technol.* **1**, 285–293 (2021).
13. L. Xi, M. Zhang, L. Zhang, T. T. S. Lew, Y. M. Lam, Novel materials for urban farming. *Adv. Mater.* **34**, 1–28 (2022).
14. F. Elfving, Ueber eine Wirkung des galvanischen Stromes auf wachsende Wurzeln. *Bot. Zeit.* **40**, 257–264 (1882).
15. A. J. Ewart, J. S. Bayliss, On the nature of the galvanotropic irritability of roots. *Proc. R. Soc. Lond., Ser. B* **77**, 63–66 (1905).
16. H. G. Stenz, M. H. Weisenseel, Electrotropism of maize (*Zea mays* L.) roots: Facts and artifacts. *Plant Physiol.* **101**, 1107–1111 (1993).
17. H. Ishikawa, M. L. Evans, Electrotropism of maize roots: Role of the root cap and relationship to gravitropism. *Plant Physiol.* **94**, 913–918 (1990).
18. W. Wawrecki, B. Zagórska-Marek, Influence of a weak DC electric field on root meristem architecture. *Ann. Bot.* **100**, 791–796 (2007).
19. M. Salvalaio *et al.*, Root electrotropism in Arabidopsis does not depend on auxin distribution but requires cytokinin biosynthesis. *Plant Physiol.* **188**, 1604–1616 (2022).
20. C. H. Bachman, M. Reichmanis, Some effects of high electrical fields on barley growth. *Int. J. Biometeorol.* **17**, 253–262 (1973).
21. C. Eing, S. Bonnet, M. Pacher, H. Puchta, W. Frey, Effects of nanosecond pulsed electric field exposure on *Arabidopsis thaliana*. *IEEE Trans. Dielectr. Electr. Insul.* **16**, 1322–1328 (2009).
22. X. Li *et al.*, Stimulation of ambient energy generated electric field on crop plant growth. *Nat. Food* **3**, 133–142 (2022).
23. B. D. Paulsen, K. Tybrandt, E. Stavrinidou, J. Rivnay, Organic mixed ionic–electronic conductors. *Nat. Mater.* **19**, 13–26 (2020).
24. E. Zeglio, A. L. Rutz, T. E. Winkler, G. G. Malliaras, A. Herland, Conjugated polymers for assessing and controlling biological functions. *Adv. Mater.* **31**, 1806712 (2019).
25. E. Stavrinidou *et al.*, Electronic plants. *Sci. Adv.* **1**, e1501136 (2015).
26. E. Stavrinidou *et al.*, In vivo polymerization and manufacturing of wires and supercapacitors in plants. *Proc. Natl. Acad. Sci. U.S.A.* **114**, 2807–2812 (2017).
27. C. Pitsalidis *et al.*, Organic bioelectronics for in vitro systems. *Chem. Rev.* **122**, 4700–4790 (2022).
28. S. Han *et al.*, Thermoelectric polymer aerogels for pressure–temperature sensing applications. *Adv. Funct. Mater.* **27**, 1–7 (2017).
29. Z. U. Khan *et al.*, Thermoelectric polymers and their elastic aerogels. *Adv. Mater.* **28**, 4556–4562 (2016).
30. A. Håkansson *et al.*, Effect of (3-glycidyloxypropyl)trimethoxysilane (GOPS) on the electrical properties of PEDOT:PSS films. *J. Polym. Sci. Part B, Polym. Phys.* **55**, 814–820 (2017).
31. A. G. Guex *et al.*, Highly porous scaffolds of PEDOT:PSS for bone tissue engineering. *Acta Biomater.* **62**, 91–101 (2017).
32. A. Malti *et al.*, An organic mixed ion-electron conductor for power electronics. *Adv. Sci.* **3**, 1–9 (2015).
33. D. Belaineh *et al.*, Controlling the organization of PEDOT:PSS on cellulose structures. *ACS Appl. Polym. Mater.* **1**, 2342–2351 (2019).
34. A. Y. Mehandzhiyski, I. Zozoulenko, Computational microscopy of PEDOT:PSS/cellulose composite paper. *ACS Appl. Energy Mater.* **2**, 3568–3577 (2019).
35. A. D. French, Idealized powder diffraction patterns for cellulose polymorphs. *Cellulose* **21**, 885–896 (2014).
36. J. Zhou, Y. Lo Hsieh, Conductive polymer protonated nanocellulose aerogels for tunable and linearly responsive strain sensors. *ACS Appl. Mater. Interfaces* **10**, 27902–27910 (2018).
37. L. Bießmann *et al.*, Highly conducting, transparent PEDOT:PSS polymer electrodes from post-treatment with weak and strong acids. *Adv. Electron. Mater.* **5**, 1–10 (2019).
38. A. V. Volkov *et al.*, Understanding the capacitance of PEDOT:PSS. *Adv. Funct. Mater.* **27**, 1–10 (2017).
39. K. Tybrandt, I. V. Zozoulenko, M. Berggren, Chemical potential–electric double layer coupling in conjugated polymer–polyelectrolyte blends. *Sci. Adv.* **3**, eaao3659 (2017).
40. M. O. Bamgbopa, J. Edberg, I. Engquist, M. Berggren, K. Tybrandt, Understanding the characteristics of conducting polymer-redox biopolymer supercapacitors. *J. Mater. Chem. A* **7**, 23973–23980 (2019).
41. G. Dijk, H. J. Ruigrok, R. P. O'Connor, PEDOT:PSS-coated stimulation electrodes attenuate irreversible electrochemical events and reduce cell electropermeabilization. *Adv. Mater. Interfaces* **8**, 1–8 (2021).
42. A. Giovannitti *et al.*, Energetic control of redox-active polymers toward safe organic bioelectronic materials. *Adv. Mater.* **32**, 1–9 (2020).
43. P. B. Tinker, P. Nye, *Solute Movement in the Rhizosphere* (Oxford University Press, New York, NY, 2000).
44. P. Nye, The rate-limiting step in plant nutrient absorption from soil. *Soil Sci.* **123**, 292–297 (1977).
45. R. Wu, B. D. Paulsen, Q. Ma, J. Rivnay, Mass and charge transport kinetics in an organic mixed ionic-electronic conductor. *Chem. Mater.* **34**, 9699–9710 (2022).
46. K. M. Miranda, M. G. Espey, D. A. Wink, A rapid, simple spectrophotometric method for simultaneous detection of nitrate and nitrite. *Nitric Oxide: Biol. Chem.* **5**, 62–71 (2001).
47. S. Han *et al.*, A multiparameter pressure–temperature–humidity sensor based on mixed ionic-electronic cellulose aerogels. *Adv. Sci.* **6**, 1802128 (2019).
48. M. Dreier, T. Peruzzi, N. Lundström, U. Bech, Improved resolution in X-ray tomography by super-resolution. *Appl. Opt.* **60**, 5783–5794 (2021).
49. R. Ballabriga *et al.*, Medipix3: A 64k pixel detector readout chip working in single photon counting mode with improved spectrometric performance. *Nucl. Instrum. Methods Phys. Res. Sect. A, Accel. Spectrom., Detect. Assoc. Equip.* **633**, S15–S18 (2011).
50. W. van Aarle *et al.*, The ASTRA Toolbox: A platform for advanced algorithm development in electron tomography. *Ultramicroscopy* **157**, 35–47 (2015).
51. W. van Aarle *et al.*, Fast and flexible X-ray tomography using the ASTRA toolbox. *Opt. Express* **24**, 25129 (2016).
52. L. A. Feldkamp, L. C. Davis, J. W. Kress, Practical cone-beam algorithm. *J. Opt. Soc. Am. A* **1**, 612 (1984).
53. B. Münch, P. Trtik, F. Marone, M. Stampanoni, Stripe and ring artifact removal with combined wavelet–Fourier filtering. *Opt. Express* **17**, 8567 (2009).
54. J. Schindelin *et al.*, Fiji: An open-source platform for biological-image analysis. *Nat. Methods* **9**, 676–682 (2012).
55. J. Gostick *et al.*, PoreSpy: A Python toolkit for quantitative analysis of porous media images. *J. Open Source Softw.* **4**, 1296 (2019).
56. N. Otsu, A threshold selection method from gray-level histograms. *IEEE Trans. Syst. Man. Cybern* **9**, 62–66 (1979).
57. H. Torquato, S. Haslach, Random heterogeneous materials: Microstructure and macroscopic properties. *Appl. Mech. Rev.* **55**, B62–B63 (2002).